

Thin granular layers are stronger, even without friction

Hugo Perrin^{1,2}, Matthieu Wyart¹, Bloen Metzger², and Yoël Forterre²

¹*Institute of Physics, Ecole Polytechnique Fédérale de Lausanne, CH-1015 Lausanne, Switzerland*

²*Aix Marseille Univ., CNRS, IUSTI, 13453 Marseille, France*

(Dated: December 23, 2024)

The jamming transition is accompanied by a rich phenomenology such as hysteretic behaviors and non-local effects. These phenomena are often considered to be interrelated. Here, we investigate experimentally a model frictionless granular layer flowing down an inclined plane. This system provides a unique opportunity to disentangle the cause-effect relationships between this phenomena and decipher their origin. We find that (i) thin frictionless granular layers are devoid of hysteresis, yet the layer stability is increased as it gets thinner. These effects are thus independent. (ii) Rheological flow rules can be collapsed into a unique master curve, supporting that non-local effects correspond to the usual finite-size effects associated to the presence of a critical point. (iii) This collapse supports that the so-called isostatic length ℓ^* governs the effect of boundaries on flow, and rules out other propositions made in the past.

Granular media close to the solid/liquid transition present a rich phenomenology such as hysteresis, finite-size or non-local effects and dilatancy, which are still much debated. Understanding these phenomena, which shape the jamming transition [1, 2], is a major challenge. All of them have strong implications in a wide range of fields such as in geophysics to predict earthquakes [3], landslides or avalanches [4, 5], in soft-matter to understand granular media [6], foams [7], and soft glassy materials [8]. So far, there is however no model to rationalize all these phenomena and unify them in a common framework. A striking example illustrating this situation is the well known fact that a layer of grains can flow down a slope of inclination θ only if its thickness h exceeds a critical value. The diversity of interpretations and models put forward to explain this property, successively attributed to dilatancy effects [9], to a diverging correlation length [10–14], to the necessary consequences of continuum descriptions [15–17], and to hysteresis [18], highlights the difficulty in addressing such problem where many effects are potentially entangled.

Recently, we have developed a model granular system in which it is possible experimentally to tune, and even eliminate, solid-friction between grains. This experimental control of the inter-particle friction opened important possibilities. For instance, it provided the mean to highlight the frictional transition at the origin of shear-thickening in dense particulate suspensions [19]. More importantly, when investigated in a rotating drum configuration, this model granular system allowed us to show that both dilatancy effects and hysteresis of the avalanche angle disappear in the absence of inter-particle friction [19, 20]. It then appears that such a system of frictionless spheres should give a unique opportunity to measure and understand the stability of granular layers and also characterize their flowing properties close to arrest, without potential interplay with hysteretic behaviors or dilatancy effects.

About two decades ago, such an ideal granular material has been studied numerically by Peynaud and Roux [21]. Since then, the investigation of frictionless particulate

systems in numerical simulations, whether in the inertial or viscous regimes, has brought major contributions to the theoretical understanding of granular and suspension flows [22–27]. From a fundamental standpoint, this model granular material bridges frictional granular flows to other amorphous frictionless systems such as foams, emulsions and glassy materials. It is thus particularly appealing as it provides the possibility to discriminate features which are specific to frictional interactions, from those more generic that emanate from collective mechanical effects.

In this paper, we investigate our model system of frictionless spheres in the inclined plane configuration. Our key findings are that (i) hysteresis, absent for a frictionless granular flow in the infinite size limit [20], is still absent in a finite-size system. By contrast, non-local effects still exist in the absence of friction, in consistency with previous observations on foams [7]. (ii) Flow rules for different angles and layer thicknesses collapse into a single master curve with a proper rescaling of variables. We explain this result from general finite size scaling arguments near a critical point [28], supporting that this language is appropriate to describe non-local effects in granular flows. (iii) This analysis supports that the length scale on which flow is affected by a boundary is the so-called isostatic length ℓ^* associated with the jamming transition [29]. Indeed, we argue that $\ell^* \sim d (\tan \theta - \tan \theta_c^\infty)^{-\alpha}$ with $\alpha = 0.83$, where θ_c^∞ is the threshold value of inclination for an infinite granular thickness. It is in good agreement with our observations $\alpha \approx 0.9$.

Experimental set-up & Protocols: We use a model frictionless granular system composed of silica spheres of diameter $d = 23.46 \pm 1.05 \mu\text{m}$. When immersed in pure water, the surface of these particles is negatively charged. Under low external stress, the resulting repulsive force [30] prevents the particles from making solid-frictional contacts. The particles then behave as frictionless spheres [19, 20]. To obtain such a behavior, the suspension must be devoid of pollutants. Prior to each experiments, the particles are thus cleaned in a piranha solution ($\text{H}_2\text{O}_2/\text{H}_2\text{SO}_4 = 1/2$ by volume)

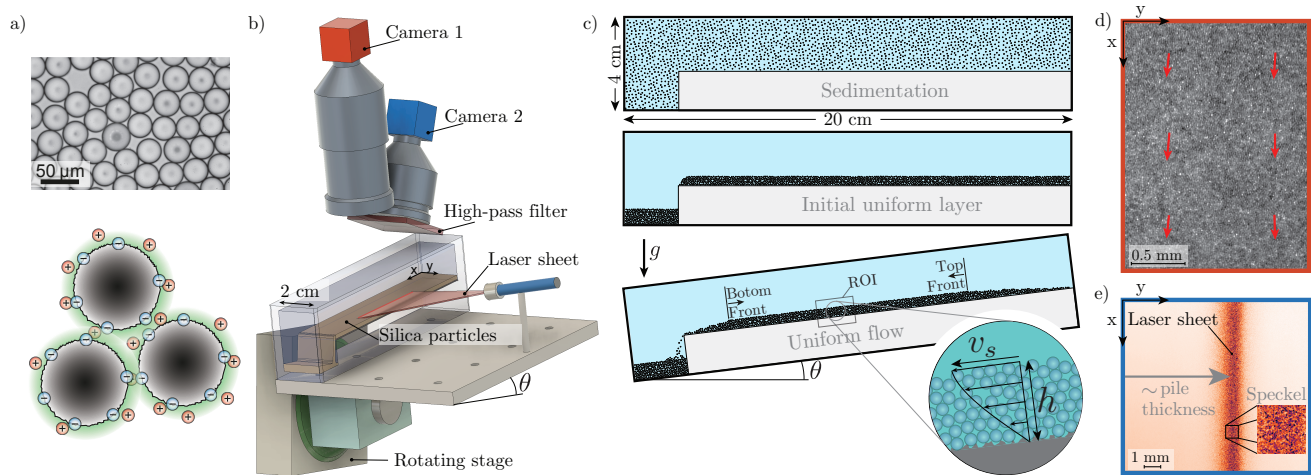


FIG. 1. Experimental set-up & Protocols. a) Top: Picture of the silica particles. Bottom: schematic of the electrostatic repulsive forces preventing frictional particle contacts. b) Schematic of the experimental set-up. c) Successive steps to prepare a uniform and pre-sheared layer of grains. d) Image from camera 1 giving access to the particle surface velocity v_s using PIV. e) Image from camera 2 used to measure the pile thickness h from the laser sheet position; and the pile stability from the time correlation of the speckle.

for 10 minutes and then rinsed thoroughly with pure water.

The set-up is shown in Figure 1.b. The inclined plane, which is covered with sand paper (Grade P500) to insure rough boundary conditions and avoid slippage, is the bottom of a parallelepipedic container of size $20 \times 4 \times 2 \text{ cm}^3$. Both the inclined-plane and the cameras are mounted on a high precision rotation stage (PI M-060), which controls the inclination angle θ . Prior to each experiment, the layer of grains is prepared following the protocol depicted in Figure 1.c. After being resuspended, the particles sediment to form a uniform layer of thickness $h \approx 30d$ on the incline. The plane is subsequently tilted at a large angle to pre-shear the suspension and we let the particles flow under gravity until the thickness of the layer reaches the desired value h , at which point, the inclination angle is set-back to zero to stop the flow. As particles flow, two fronts form at the bottom and at the top of the incline, see Figure 1.b. However, all measurements are performed in the region of interest (ROI) which is far from these two fronts and where the flow is assumed to be uniform.

To determine the rheology of the flowing layer of grains, we use the fact that in the present configuration, the suspension friction coefficient μ is homogeneous across the layer thickness and is simply given by the relation $\mu = \tan \theta$ [19]. Moreover, by imaging the layer surface, camera 1 gives access to the grains surface velocity v_s using PIV [Figure 1.d], and camera 2 tracks the transverse position of the inclined laser sheet [Figure 1.e], thereby giving access to the layer thickness h , with an absolute resolution of $\pm 2.5 \mu\text{m}$. By integrating the flow profile assuming a homogeneous viscous number defined as $J = \eta \dot{\gamma} / P$, where η is the viscosity of the fluid, $\dot{\gamma}$ is the shear rate and P the particle pressure, these

two measurements give access to the viscous number by $J = 2\eta v_s / h^2 \phi \Delta \rho g \cos \theta$, where $\Delta \rho = 850 \text{ kg.m}^{-3}$ is the density difference between the particles and the suspending fluid, and ϕ denotes the layer particle volume fraction. Here, measurements are performed in the limit of small viscous number $J \leq 10^{-3}$; the volume fraction is thus assumed to be constant and given by the maximum packing of frictionless spheres $\phi = 0.64$.

To characterize the stability of the flow and potential hysteretic behaviors of the avalanche angle, we need a quantitative way to discriminate whether, for a given angle θ , the layer of grains is flowing or at rest. This constitutes a real experimental challenge as the overdamped dynamics of the grains can be very slow and involve transients lasting several hours. Since our PIV measurements can only resolve grain velocities of the order $0.1 \mu\text{m/s}$, we developed a more sensitive speckle correlation technique [31]. The coherent laser light, when shined onto the granular layer composed of transparent beads, scatters randomly and produces a speckle [Figure 1.e]. Tiny movements of the particles are sufficient to change the optical path of the light, which sensibly decorrelates the speckle. From successive images of camera 2, separated by a delay of $\Delta t = 0.1 \text{ s}$, we thus compute C , the space-averaged time correlation of the speckle, see details in [32]. For a layer of grains at rest, the correlation is slightly below 1 due to the intrinsic numerical noise of the camera. Its value is $C \approx 0.98$ with a typical noise of ± 0.01 . Flow can therefore be detected as soon as $C \leq C_{th} = 0.96$, which corresponds qualitatively to an average surface velocity of 0.5 nm/s .

Finite-size effects on hysteresis and stability? To probe the potential emergence of hysteresis in a finite size system, we developed the dichotomy procedure shown

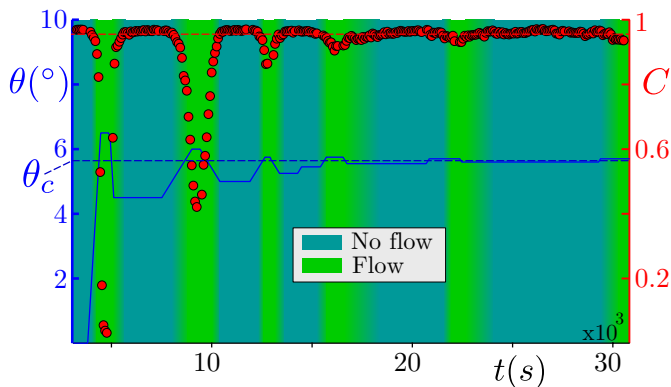


FIG. 2. Dichotomy procedure. Controlled inclination angle θ (in blue) and resulting speckle correlation C (in red) versus time for a layer of thickness $h/d \simeq 22$. Red-dashed line: $C_{\text{th}} = 0.96$ delimiting flow ($C < C_{\text{th}}$) from arrest ($C > C_{\text{th}}$). Blue-dashed line: critical stability angle $\theta_c(h/d)$.

in Figure 2. Starting from a pre-sheared granular layer having the desired thickness h , the inclination angle θ is rapidly increased to 6.5° and kept to a constant value. As shown in Figure 2, the speckle correlation C drops much below C_{th} (Red-dashed line) indicating that the granular layer starts flowing. The angle of inclination θ is then successively decreased and increased in order to determine and gradually refine the frontier between flow and arrest. Importantly, the flow rates involved here are sufficiently small that during the whole dichotomy procedure, the layer thickness remains constant. The experiment is repeated for different initial layer thicknesses ranging from $h/d \simeq 22$ to $h/d \simeq 1$ and each time as illustrated in Figure 2, the dichotomy converges to a unique critical inclination angle $\theta_c(h/d)$ (Blue-dashed line), determined with a resolution of $\pm 0.05^\circ$. These results show that a layer of frictionless particles, whether initially flowing or at rest, stops or starts flowing at a unique critical angle $\theta_c(h/d)$ – the proof that no hysteresis of the avalanche angle is observed in frictionless granular systems, even of finite-size.

Furthermore, the above dichotomy provides an accurate estimate of the critical stability angle θ_c for different layer thickness h/d . We thus obtain the stability diagram shown in Figure 3. For granular layers of thickness larger than $10d$, the critical stability angle is nearly constant $\theta_c^\infty \simeq 5^\circ$ and in good agreement with previous experimental (6° in [20]) and numerical results (5.73° in [21]) obtained for frictionless systems in the infinite size limit. For thinner layers however, the critical stability angle θ_c increases and fitting the law

$$h/d = ((\tan \theta_c - \tan \theta_c^\infty)/a)^{-\alpha}, \quad (1)$$

yields $\alpha = 0.9 \pm 0.1$, $a = 0.15$ and $\theta_c^\infty = 5.0^\circ$. These results show that, conversely to hysteresis, finite-size effects are still in play and significantly impact the granular layer stability.

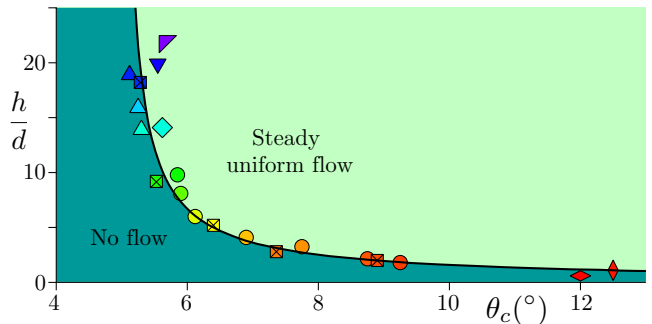


FIG. 3. Stability diagram. Granular layer thickness h/d versus critical stability angle θ_c . Different open-markers indicate different runs, where the cleaning procedure and system aging induce an uncertainty on θ_c of the order of 0.5° . Crossed-markers correspond to the quasi-static friction coefficient obtained from the best fit of $\mu(J, h/d)$ in Figure 4. Black-line: best fit with $h/d = ((\tan \theta_c - \tan \theta_c^\infty)/a)^{-\alpha}$ yielding $\alpha = -0.9 \pm 0.1$, $a \simeq 0.15$ and $\theta_c^\infty \simeq 5.0^\circ$.

Finite-size effects on flow rules: To further investigate finite-size effects, we then studied how they influence the granular layer dynamic flowing properties, with the aim to obtain constitutive flow rules of the form $\mu(J, h/d)$. A great advantage of the experimental set-up is that, during a measurement, the rotation stage allowed us to vary the inclination angle θ , and thus $\mu = \tan \theta$, in a controlled way. It is then possible to chose a layer thickness h , and measure J while imposing a quasi-static decreasing ramp of μ . This protocol provides the full rheological law $\mu(J, h/d)$ for a given value of h/d in a single measurement. It must however be limited to slow flows (*i.e.* $J < 10^{-3}$) for which the decrease of the layer thickness remains negligible, *i.e.* not exceeding $0.5d$ during the ramp-down. We have checked that steady state measurements provide the same results.

The rheological laws $\mu(J, h/d)$ are shown in Fig.4 for various layer thickness h/d and for a wide range of J . We find that the system finite-size has an overall significant effect on the flow rules. The large system ($h/d \simeq 18.2$) exhibits a power law with an exponent of 0.38, in close agreement to the exponents measured experimentally in a rotating drum (0.37 ± 0.05 [20]) and derived theoretically ($\beta = 0.35$ [27]) for frictionless spheres in the infinite size limit. Together with Fig.3 and Eqn. 1, these observations support the two following asymptotic regimes:

$$\mu(J \rightarrow 0, h/d) \sim \mu_c^\infty + a(h/d)^{-1/\alpha}, \quad \text{and} \quad (2)$$

$$\mu(J, h/d \rightarrow \infty) \sim \mu_c^\infty + bJ^\beta. \quad (3)$$

To rationalise the observed behavior of $\mu(J, h/d)$ for generic arguments, we make the usual finite size scaling assumption valid near a critical point [28]. In this view, J is the order parameter controlled by the excess macroscopic friction $\Delta\mu \equiv \mu - \mu_c^\infty$ and system size h :

$$J(\Delta\mu, h) = \Delta\mu^{1/\beta} f(h/\xi(\Delta\mu)) \quad (4)$$

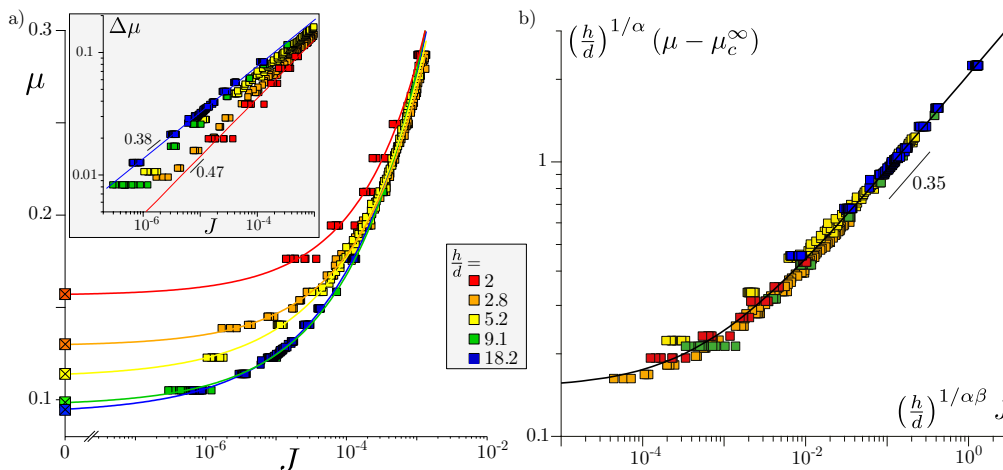


FIG. 4. Finite-size effects on the flow rules of a frictionless granular layer. a) Macroscopic friction coefficient μ versus viscous number J for different layer thicknesses h/d . Solid-lines: best fits with $\mu = \mu_c + bJ^\beta$. The asymptotic value of μ obtained when $J \rightarrow 0$ (Crossed-squares) are reported in Figure 3. Inset: Same data plotting the reduced macroscopic friction $\Delta\mu = \mu - \mu_c(h/d)$ versus J . b) Same data plotting $(h/d)^{1/\alpha}(\mu - \mu_c^\infty)$ versus $(h/d)^{1/\alpha\beta}J$. Black-line: $g(x) = a + (cx^\gamma)(bx^\beta)/(bx^\beta + cx^\gamma)$, with $a = 0.15$, $\beta = 0.35$, $b = 2.0$, $c = 29$ and $\gamma = 0.73$.

where f is some scaling function and $\xi(\Delta\mu)$ is a diverging length scale. Fig.3 implies that this length follows $\xi(\Delta\mu) = d\Delta\mu^{-\alpha}$. Using this result and simple manipulations, we can rewrite Eq.4 as:

$$\Delta\mu(J, h) = (h/d)^{-1/\alpha} g\left((h/d)^{1/\alpha\beta} J\right) \quad (5)$$

where g is some function. This result implies that the data of Fig.4.a should collapse on a single curve by rescaling properly both axis. Remarkably, the collapse shown in Fig.4.b is excellent, without any fitting parameters (since β is theoretically predicted and α extracted from Fig.3). This description unifies both flow properties and arrest. Quantitatively, we find that the scaling function g is well-approximated by $g(x) = a + \frac{bcx^{\gamma+\beta}}{bx^\beta + cx^\gamma}$ with $b = 2.0$, $c = 29$ and $\gamma = 0.73$ (Black-line in Figure 4.b).

Diverging length scale: We now propose an explanation for the exponent $\alpha \approx 0.9$ characterising the extension of non-local effects in granular flows. We use two facts: (i) in packing of particles, fixing a boundary on a length scale h constrains the material, and is equivalent to changing the particle coordination z by an amount $\sim d/h$ (the ratio of surface to volume of the system [33]). This idea justifies the existence of a diverging "isostatic" length scale $\ell^* \sim d/|\delta z|$ (where $\delta z = z - z_c^\infty$ and z_c^∞ is the threshold "isostatic" coordination where the infinite system rigidifies [34]) that controls both the elasticity of over-constrained materials [29], and the scale on which pinning boundaries rigidify a floppy, under-constrained system [35]. We posit that this is also the length scale on which a granular flow is affected by the presence of a boundary. (ii) In flowing systems of hard frictionless particles, increasing the macroscopic friction breaks more contact and reduces the coordination. The

microscopic theory of [27] predicts $\Delta\mu^{0.83} \sim |\delta z|$ both for over-damped and inertial flows, in good agreements with numerics. Putting these two results together, we obtain that jamming will occur when the added constraints from the boundary balance the degrees of freedom of the bulk, leading to $\ell^* \sim d\Delta\mu^{-0.83}$ or $\alpha = 0.83$, in close agreement with our observation. Note that another popular length scale that diverges near jamming, $\ell_c \sim d/\sqrt{|\delta z|}$ [36] that characterizes the response to a point perturbation [35], is ruled out as it would lead to $\alpha = 0.41$ incompatible with our data.

Discussion: In this paper, we have shown experimentally that a finite-size frictionless granular layer is devoid of hysteresis: a granular layer of thickness h/d stops or starts flowing at unique critical stability angle $\theta_c(h/d)$. Nonetheless, thinner layers are more stable indicating that finite-size effects are still in play. These findings highlight that no hysteretic behaviors emerge from finite-size effects; hysteresis and finite-size effects are thus independent phenomenologies. The absence of hysteresis for a frictionless granular layer, observed both in infinite [20] and finite size systems, highlights that hysteresis of the avalanche angle is a feature entirely rooted to the presence of inter-particle friction.

Moreover, we provided the first stability diagram for a frictionless granular layer [Figure 3]. The critical stability angle follows $h/d \sim (\tan\theta_c - \tan\theta_c^\infty)^{-\alpha}$ with $\alpha \approx 0.9$ (Eqn. 1). Interestingly, the same empirical law fits very well previous results, also obtained on an inclined plane but with inertial frictional particles [10, 37]. Clearly, our results reject mechanisms based on dilatancy effects as frictionless granular layers are not dilatant [21]. Non-local models are able to capture the existence of a critical stability angle that depends on the layer thickness, but

fail to predict the power law exponent $\alpha \approx 1$ [17]. Our experimental work thus called for a new coherent explanation. Here we have argued that non-local effects are a necessary consequences of the finite-size effects near a critical point, justifying the remarkable collapse of flow curves for different thicknesses on a single master curve. The extracted diverging length scale is consistent with the isostatic length scale following $\ell^* \sim d\Delta\mu^{-0.83}$, which we predict should also hold for inertial systems.

Future works should specify the microscopic processes by which a frozen boundary affects the flow, which our scaling analysis does not specify. Such a theory would ideally predict the flow profile as well as how the average coordination varies in the vertical direction. Another key question is the generalisation of these results to the frictional case. In [38] it was argued that the role of excess coordination in frictionless particles is then replaced by

the fraction of sliding contact for frictional ones. The latter appears to be proportional to $\Delta\mu$. Following the derivation of the length scale above, we would then obtain $\alpha = 1$ which is consistent with observations [10, 37].

ACKNOWLEDGMENTS

We thank M. Bouzid, O. Pouliquen and S. Mandal for discussions, S. Noël for building the incline. This work was supported by the European Research Council under the European Union Horizon 2020 Research and Innovation programme (ERC grant agreement No. 647384), by the French National Research Agency under the project ANR *ScienceFriction* (ANR-18-CE30-0024), by the Swiss National Science Foundation for support under Grant No. 200021-165509 and the Simons Foundation Grant (No. 454953 Matthieu Wyart).

-
- [1] C. S. O’Hern, L. E. Silbert, A. J. Liu, and S. R. Nagel, *Phys. Rev. E* **68**, 011306 (2003).
 - [2] P. Olsson and S. Teitel, *Phys. Rev. Lett.* **99**, 178001 (2007).
 - [3] J. Leeman, D. Saffer, M. Scuderi, and C. Marone, *Nature communications* **7**, 1 (2016).
 - [4] A. Lucas, A. Mangeney, and J. P. Ampuero, *Nature communications* **5**, 1 (2014).
 - [5] B. Ferdowsi, C. P. Ortiz, and D. J. Jerolmack, *Proceedings of the National Academy of Sciences* **115**, 4827 (2018).
 - [6] Y. Forterre and O. Pouliquen, *Annu. Rev. Fluid Mech.* **40**, 1 (2008).
 - [7] R. Lespiat, S. Cohen-Addad, and R. Höhler, *Physical review letters* **106**, 148302 (2011).
 - [8] J. Goyon, A. Colin, and L. Bocquet, *Soft Matter* **6**, 2668 (2010).
 - [9] O. Pouliquen and N. Renaut, *Journal de Physique II* **6**, 923 (1996).
 - [10] O. Pouliquen, *Physics of fluids* **11**, 542 (1999).
 - [11] D. Ertas and T. C. Halsey, *EPL (Europhysics Letters)* **60**, 931 (2002).
 - [12] P. Mills, P. Rognon, and F. Chevoir, *EPL (Europhysics Letters)* **81**, 64005 (2008).
 - [13] L. Staron, *Physical Review E* **77**, 051304 (2008).
 - [14] T. Gueudré, J. Lin, A. Rosso, and M. Wyart, *Soft Matter* **13**, 3794 (2017).
 - [15] I. S. Aranson and L. S. Tsimring, *Physical Review E* **65**, 061303 (2002).
 - [16] M. Bouzid, M. Trulsson, P. Claudin, E. Clément, and B. Andreotti, *Physical review letters* **111**, 238301 (2013).
 - [17] K. Kamrin and D. L. Henann, *Soft matter* **11**, 179 (2015).
 - [18] A. Edwards, A. Russell, C. Johnson, and J. Gray, *Journal of Fluid Mechanics* **875**, 1058 (2019).
 - [19] C. Clavaud, A. Béruit, B. Metzger, and Y. Forterre, *Proceedings of the National Academy of Sciences* **114**, 5147 (2017).
 - [20] H. Perrin, C. Clavaud, M. Wyart, B. Metzger, and Y. Forterre, *Physical Review X* **9**, 031027 (2019).
 - [21] P.-E. Peyneau and J.-N. Roux, *Phys. Rev. E* **78**, 011307 (2008).
 - [22] G. Combe and J.-N. Roux, *Physical Review Letters* **85**, 3628 (2000).
 - [23] E. Lerner, G. Düring, and M. Wyart, *Proceedings of the National Academy of Sciences* **109**, 4798 (2012).
 - [24] S. Gallier, E. Lemaire, F. Peters, and L. Lobry, *Journal of Fluid Mechanics* **757**, 514 (2014).
 - [25] R. Mari, R. Seto, J. F. Morris, and M. M. Denn, *Journal of Rheology* **58**, 1693 (2014).
 - [26] M. Wyart and M. Cates, *Physical review letters* **112**, 098302 (2014).
 - [27] E. DeGiuli, G. Düring, E. Lerner, and M. Wyart, *Physical Review E* **91**, 062206 (2015).
 - [28] J. Cardy, *Finite-size scaling* (Elsevier, 2012).
 - [29] M. Wyart, S. R. Nagel, and T. A. Witten, *EPL (Europhysics Letters)* **72**, 486 (2005).
 - [30] J. N. Israelachvili, *Intermolecular and surface forces* (Academic press, 2011).
 - [31] M. Erpelding, A. Amon, and J. Crassous, *Phys. Rev. E* **78**, 046104 (2008).
 - [32] C is the spatial average of the correlation matrix $M = \frac{\langle I(0)I(\Delta t) \rangle - \langle I(0) \rangle \langle I(\Delta t) \rangle}{\sqrt{\langle I(0)^2 \rangle - \langle I(0) \rangle^2} \sqrt{\langle I(\Delta t)^2 \rangle - \langle I(\Delta t) \rangle^2}}$, where $I(0)$ and $I(\Delta t)$ are two images separated by a time interval Δt and $\langle \cdot \rangle$ denotes a spatial average over boxes of 4×4 pixels, see [31] for details.
 - [33] A. V. Tkachenko and T. A. Witten, *Physical review E* **60**, 687 (1999).
 - [34] J. C. Maxwell, *The London, Edinburgh, and Dublin Philosophical Magazine and Journal of Science* **27**, 294 (1864).
 - [35] G. Düring, E. Lerner, and M. Wyart, *Soft Matter* **9**, 146 (2013).
 - [36] L. E. Silbert, A. J. Liu, and S. R. Nagel, *Physical review letters* **95**, 098301 (2005).
 - [37] M. Wyart, *EPL (Europhysics Letters)* **85**, 24003 (2009).
 - [38] E. DeGiuli and M. Wyart, *Proceedings of the National Academy of Sciences* **114**, 9284 (2017).